Corona-Directed Nucleic Acid Delivery into Hepatic Stellate Cells for Liver Fibrosis Therapy

Zhengping Zhang,[†,§] Chunming Wang,[‡,§] Yinhe Zha,[†] Wei Hu,[†] Zhongfei Gao,[†] Yuhui Zang,[†] Jiangning Chen,[†] Junfeng Zhang,[*,†] and Lei Dong[*,†]

[†]State Key Laboratory of Pharmaceutical Biotechnology, School of Life Sciences, Nanjing University, Nanjing 210093, China and [‡]State Key Laboratory of Quality Research in Chinese Medicine, Institute of Chinese Medical Sciences, University of Macau, Taipa, Macau SAR, China. [§]These authors contributed equally to the work.

ABSTRACT Strategies to modify nanoparticles with biological ligands for targeted drug delivery *in vivo* have been widely studied but met with limited clinical success. A possible reason is that, in the blood circulation, serum proteins could rapidly form a layer of protein "corona" on the vehicle surface, which might block the modified ligands and hamper their targeting functions. We speculate that strategies for drug delivery can be designed based upon elegant control of the corona formation on the vehicle surfaces. In this study, we demonstrate a retinol-conjugated polyetherimine (RcP) nanoparticle system that selectively recruited the retinol binding protein 4 (RBP) in its corona components. RBP was found to bind retinol, and direct the antisense oligonucleotide (ASO)-laden RcP carrier to hepatic stellate cells (HSC), which play essential roles in the progression of hepatic fibrosis. In both mouse fibrosis models, induced by carbon tetrachloride (CCl_4) and bile duct ligation (BDL), respectively, the ASO-laden RcP particles effectively suppressed the expression of type I collagen (collagen I), and consequently ameliorated hepatic fibrosis. Such findings suggest that this delivery system, designed to exploit the power of corona proteins, can serve as a promising tool for targeted delivery of therapeutic agents for the treatment of hepatic fibrosis.

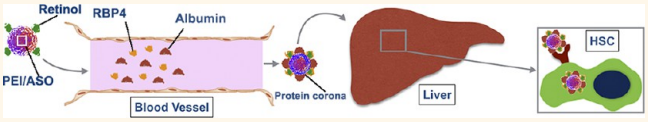

KEYWORDS: protein corona · targeted delivery · retinol · drug nanocarriers · hepatic fibrosis

Nanoparticles modified with biological ligands are emerging tools for targeted drug delivery. Such ligands can recognize specific cell receptors and thereby direct the drug-laden nanocarriers to the target tissue.[1,2] This strategy has widely been tested *in vitro*, but has met with limited success *in vivo*. To date, very few ligand-modified nanoparticles have entered clinical trials.[3] A possible reason behind such disappointment is that, in the physiological system, the modified surface of the nanoparticles is further covered by a layer of proteins from the biological fluid, known as protein corona.[4] This corona layer may hide the ligands from interacting with cell receptors. The behavior and fate of the nanoparticles would be dictated by the corona components, instead of the ligands conjugated on the particle surface. As a result, these vehicles might lose their targeting functions.[5,6]

This challenge, on the other hand, motivated us to design new strategies for targeted drug delivery. Recent studies have evidenced that biomolecular corona formed on nanoparticles may trigger cells to uptake such nanoparticle-corona complexes,[7] More importantly, surface modification of a nanoparticle with certain molecules could even change the structure of some corona proteins, enabling "new" recognition between the modified particle and cells.[8] We could possibly control the formation of corona by recruiting certain proteins to its component, and then exploit the physiological functions of these proteins for tissue/cell-targeting purposes. For example, in the blood plasma, numerous proteins are native and efficient transporters, and play versatile roles in nutrient transportation in the body.[9] They bind specific molecules in the circulation and deliver them to the destination.[10,11] And depletion of them directly abolishes or decreases specific recognition between the delivered molecules and their specific cell receptors.[12,13] We hypothesized that these naturally circulating proteins could be recruited from the plasma into the corona

* Address correspondence to leidong@nju.edu.cn, jfzhang@nju.edu.cn.

Received for review June 3, 2014 and accepted January 14, 2015.

Published online January 14, 2015
10.1021/nn505166x

© 2015 American Chemical Society

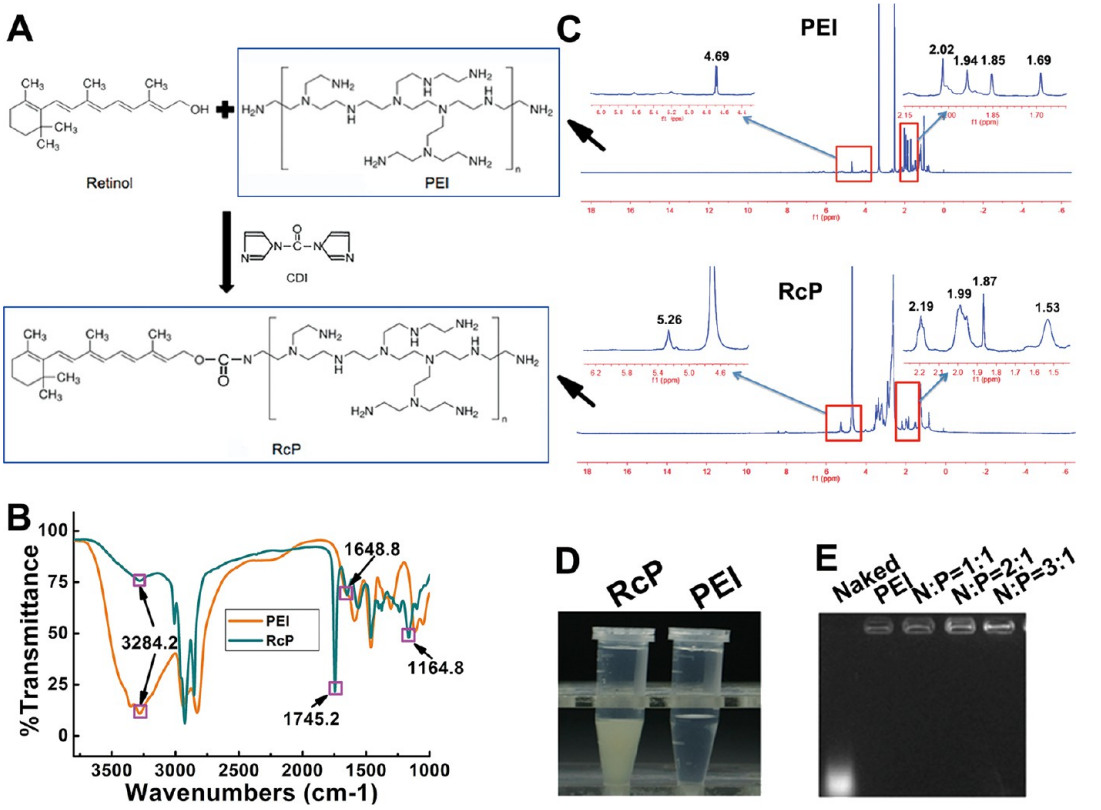

Figure 1. Preparation and characterization of RcP. (A) Schematic diagram showing the covalent coupling of PEI (1.3 kDa) to retinol *via* the CDI-activation method. (B) The FT-IR spectra of PEI and Retinol-c-PEI. (C) NMR spectrum of PEI and RCP. (D) Representative images of RcP and PEI in PBS. (E) Gel retardation assay of RcP/DNA, where N/P represents the molar ratio of $M_{\text{Retinol-c-PEI}}/M_{\text{DNA}}$.

on the nanocarrier surface, and these corona proteins can exhibit their native functions in directing the drug vehicles to the specific tissue sites.

In our present study, we demonstrate a nanoparticle drug carrier that facilitates the formation of corona composed of native transport proteins. Specifically, we conjugated retinol molecules with low molecular weight polyethylenimine (PEI), which further combined nucleotides to form nanoparticles. This nanoparticle system actively recruited plasma proteins and in particular, RBP, to form corona on the surface.[14] In a CCl_4-induced murine liver fibrosis model, the RBP/retinol complex successfully directed the nanoparticle into the hepatic stellate cell (HSC), which functions as retinol-storing cells in healthy individuals but fibrogenic cells in hepatic fibrosis patients. Delivery of an antifibrogenic antisense oligonucleotide with this system achieved high targeting efficiency into HSCs and exhibited remarkable therapeutic performances.

RESULTS

Synthesis and Characterization of RcP. PEI was conjugated to the hydroxyl groups of retinol by the CDI activation method to produce RcP (Figure 1A). Successful conjugation was evidenced by FT-IR (Figure 1B) and NMR (Figure 1C). In the IR spectra, the peak at 1745.2 cm^{-1} indicates the combined signals of carbonyl group and the amino link, the signal reduction at 3284.2 cm^{-1} suggests that many amine groups in PEI have been linked to retinol, and signal changes at 1648.8 and 1164.8 cm^{-1} imply the modification of both the secondary and tertiary amines in PEI (Figure 1B). In the NMR spectra, the shift from δ 4.69 ppm (PEI) to δ 5.25 ppm (RcP) could be attributed to the signals of the hydrogens on the $-CH_2-CH_2-NH_2$ arms (Figure 1C).

The product, RcP, is an amphiphilic polymer consisting of hydrophobic retinol and hydrophilic PEI. The hydrophobic retinol part should be on the surface because RcP presented in a uniform emulsion in water (Figure 1D). Gel electrophoresis demonstrated that the mobility of DNA was retarded when the N/P ratio (the ratios of moles of the amine groups of PEI to those of the phosphate ones of ASO) exceeded 1, suggesting the efficient combination of DNA by the RcP complex (Figure 1E).

Preparation and Characterization of RcP/ASO Particle (RAP). We next prepared the RAP, using the PEI block of the RcP molecules to combine ASO. In order for albumin and RBP to maintain their native transportation function, the PEI must not perturb the proteins' native conformation. We compared the influence of PEI with two different molecular sizes (25 and 1.3 kDa) on the surface charge of albumin (Figure 2A).

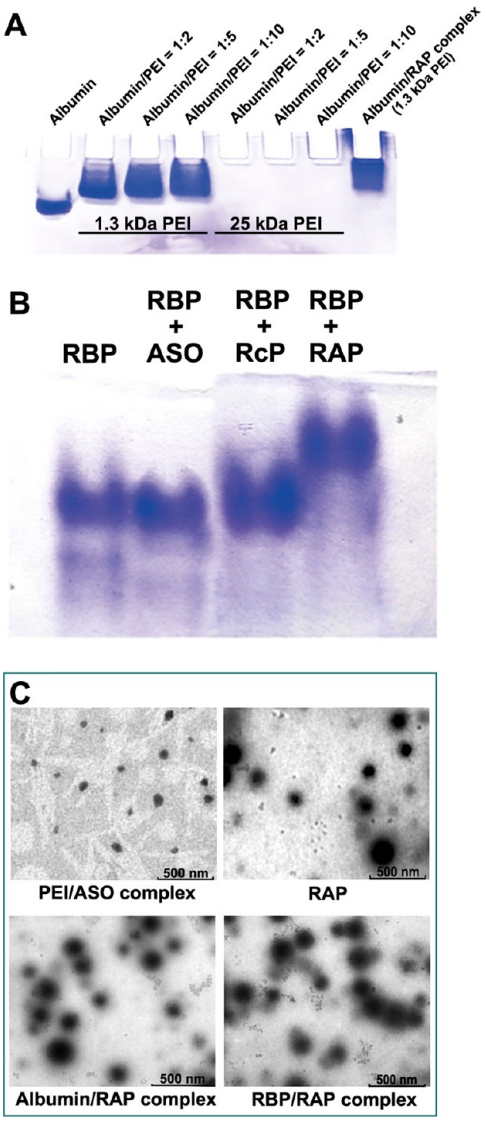

Figure 2. Characterization of RAP and its association with albumin and RBP. (A) Native-PAGE analysis of Albumin, Albumin preincubated with RAP, and Albumin preincubated with PEI with different molecular weight, where Albumin/PEI represents the molar ratio of albumin and PEI. The albumin bands were stained with Coomassie brilliant blue. (B) Native-PAGE analysis of recombinant mouse RBP, RBP preincubated with ASO, RBP preincubated with RcP, and RBP/RAP complex. The RBP bands were stained with Coomassie brilliant blue. (C) Representative TEM images of PEI/ASO complex, RAP, Albumin/RAP complex, and RBP/RAP complex. All the particles were stained with phosphomolybdic acid. All images presented were representative of three independent results.

After incubation, the 25 kDa PEI completely changed the surface charge of albumin from negative to positive. The complex migrated toward the opposite direction in the native-PAGE, and thus no band could be detected. Meanwhile, the 1.3 kDa PEI, even used at a very high dose (Albumin/PEI = 1:10), posed little influence on the surface charge of albumin except moderately decreasing the migration of the protein. Hence, we chose the 1.3 kDa PEI for the RcP preparation and the following experiments in this study.

TABLE 1. Particle Size and Zeta Potential of the Particles

particle	particle size (nm)	PDI	zeta potential (mV)
PEI/ASO complex	115 ± 14.3	0.26	+ 18.9 ± 2.6
RAP	383 ± 23.1	0.31	+15.5 ± 0.7
Albumin/PEI/ASO complex	208 ± 17.3	0.32	−0.2 ± 0.04
Albumin/RAP complex	231 ± 24.6	0.38	−5.5 ± 0.3
RBP/RAP complex	291 ± 19.7	0.29	−6.1 ± 0.6
Serum-incubated RAP	240 ± 29.7	0.35	- 5.2 ± 0.4

Indeed, in the final Albumin/RAP complex, the 1.3 kDa PEI preserved the charge of albumin well (the last lane, Figure 2A).

RAP could also bind RBP to form a new RBP/RAP complex, because RAP contains retinol that is a natural ligand for RBP. We performed native PAGE, and found that RBP in association with RAP migrated slower than the free RBP (Figure 2B), which confirmed the formation of RBP/RAP complex.

We then determined the particle size, PDI and zeta potential of PEI/ASO complex, RAP, Albumin/RAP complex, and RBP/RAP complex by dynamic light scattering (DLS) (Table 1). Retinol modification, from PEI/ASO complex to RAP, increased the particle size but did not influence its zeta potential. Combination with albumin (Albumin/RAP complex) or RBP (RBP/RAP complex) decreased the size of RAP by over 30%, probably because the proteins decreased the surface hydrophobicity and aggregation of the complex, and switched the surface charge from positive to negative. Meanwhile, in the control group, association with albumin increased the size and decreased the surface charge of the PEI/ASO complex. The formation of protein corona around the Albumin/RAP complex and RBP/RAP complex was further confirmed by transmission electron microscopy (TEM) (Figure 2C).

Analysis of the Protein Corona Formed on RAPs in Serum. Because the system was designed to be administrated in the circulation, we next analyzed which proteins in the serum could form corona on the nanocomplexes. Serum proteins could interact with the vehicles *via* either specific or nonspecific interactions. For example, both albumin, as the most abundant serum protein, and RBP, which specifically binds retinol, could be components of the corona on RAP. After determining the particle size and surface charge by DLS (Table 1) and visualizing the corona formation by TEM (Figure 3A), we recovered the corona proteins from RAP, subjected them to the sodium dodecyl sulfate-polyacrylamide gel electrophoresis (SDS-PAGE) analysis, and found their bands very different from those obtained from PEI/ASO complex (as control; Figure 3B). Further analysis with LC−MS revealed that RAP and PEI/ASO complex associated with 232 and 163 serum proteins, respectively. Of these proteins, 118 appeared on both particles and 159 were on one side only (Figure 3C). We then compared the 20 most abundant proteins on

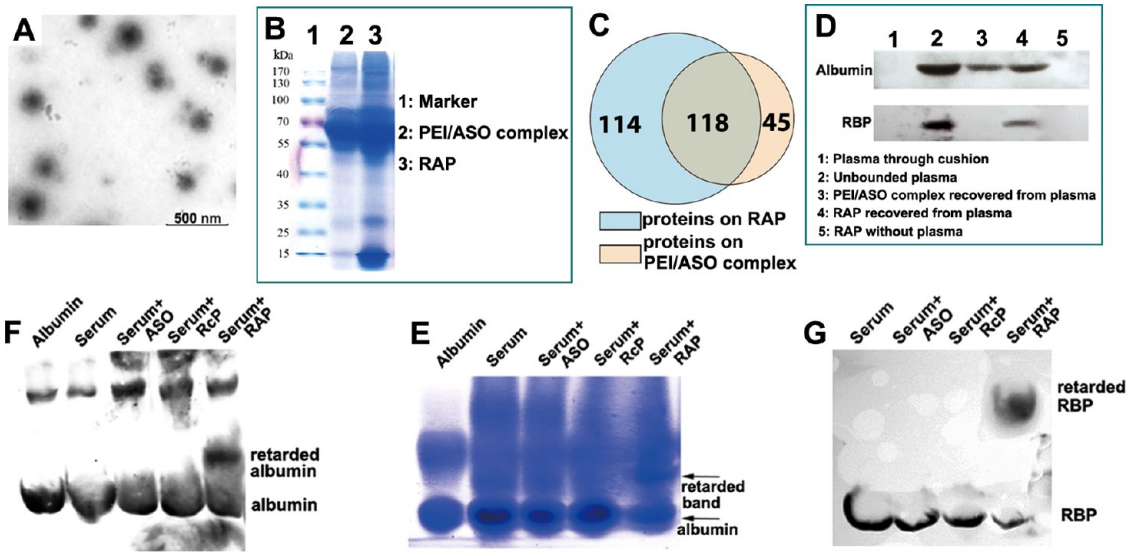

Figure 3. Analysis of the protein corona formed on RAP in serum. (A) The TEM images of RAP/corona complex formed in serum. (B) SDS-PAGE analysis of the proteins associated with PEI/ASO complex and RAP. The bands were stained with Coomassie brilliant blue. (C) The total number of protein types associated with PEI/ASO complex or RAP, as analyzed by LC−MS. (D) Western blotting analysis of albumin and RBP in the proteins recovered from coronas on PEI/ASO complex or RAP formed in bovin serum. (E) Native-PAGE analysis of the bovine serum proteins mixed with RAP. The bands were stained with Coomassie brilliant blue. (F and G) Native-PAGE Western blotting analysis of albumin (F) and RBP (G) in serum incubated with RAP. All images presented were representatives of three independent results.

TABLE 2. Top 20 Most-Abundant Corona Proteins on Different Nanoparticles and RBP on PEI/ASO Complex Analyzed by LC−MS[a]

No.	RAP	PEI/ASO complex
1	Serum albumin	Serum albumin
2	Alpha-2-macroglobulin	Serotransferrin
3	Apolipoprotein B-100	Alpha-2-macroglobulin
4	Fibronectin	Complement C3
5	Complement C3	Ceruloplasmin
6	Murinoglobulin-1	Complement C4-B
7	Serotransferrin	Hemopexin
8	Retinol-binding protein 4	Alpha-1-antitrypsin 1-4
9	Coagulation factor V	Plasminogen
10	Ceruloplasmin	Vitamin D-binding protein
11	Plasminogen	Inhibitor of carbonic anhydrase
12	Complement C4-B	Murinoglobulin-1
13	Alpha-1-antitrypsin 1-4	Serine protease inhibitor A3K
14	Inter-alpha-trypsin inhibitor heavy chain H1	Inter alpha-trypsin inhibitor, heavy chain 4
15	Prothrombin	Kininogen-1
16	Complement factor H	Gelsolin
17	Vitamin D-binding protein	Antithrombin-III
18	Hemopexin	Alpha-2-HS-glycoprotein
19	Inter-alpha trypsin inhibitor, heavy chain 2	Isoform 2 of Leukemia inhibitory factor receptor
20	Inter alpha-trypsin inhibitor, heavy chain 4	Protein Gm20547
	...	...
136	Serotransferrin	Retinol-binding protein 4

[a] Proteins highlighted in the darker blue are among the top 20 for both indicated nanoparticles. Retinol-binding protein 4 (RBP) was highlighted in a yellow grid.

PEI/ASO complex and RAP particles (Table 2), and found RBP in much higher content in RAP than in PEI/ASO complex samples. This finding was in agreement with the outcomes from the Western blotting

analysis, which detected albumin in both RAP and PEI/ASO complex corona samples but RBP only in the RAP group (Figure 3D).

To further evaluate albumin and RBP as corona components in their natural state, we performed native PAGE followed by Coomassie blue staining and Western blotting. Gel staining indicated that RAP decreased the motility of RAP-associated proteins in the native gel (Figure 3E). Western blotting using antibodies against albumin and RBP demonstrated that the retarded migration of albumin (Figure 3F) and RBP (Figure 3G) by RAP particles. These results suggest that both proteins could be associated with RAP in their native states.

It might be a concern that formation of corona could bring about an adverse biological effect to the nanoparticles, thereby compromising the safety level of the vehicles. Therefore, we tested the toxicity of the PEI/ASO complex and RAP complexes both *in vitro* and *in vivo*. In the *in vitro* cytotoxicity test, PEI/ASO complex consisting of either 25 or 1.3 kDa PEI exhibited high cell toxicity, while RAP had little influence on cell viability (Supporting Information Figure S1A). Once administered *in vivo* through the tail vein, PEI/ASO complex caused immediate death of the mice, while RAP started to present *in vivo* toxicity only when given at a very high dose (Supporting Information Figure S1B). The acute death caused by PEI was probably due to the coagulation in the main blood vessels. Hence, we compared the procoagulant capabilities of PEI/ASO complex and RAP, by determining the blood-clotting indicators prothrombin time and activated partial thromboplastin time. We found that PEI (both 1.3 and 25 kDa) substantially accelerated blood coagulation (and the 25 kDa PEI had stronger effect), while RAP did not show any significant pro- or anticoagulation effects (Supporting Information Table S1).

***In Vitro* Transfection of RAP.** We first tested the transfection effects of RAP to HSCs primarily derived from the fibrotic mice liver. We employed a fluorescent ASO, a FAM (6-carboxyfluorescein) conjugated ASO as reporter, and set PEI/ASO complex as control because PEI was an established carrier for nucleic acid drugs. Results in Figure 4A demonstrated that in serum-containing media, RAP had much higher transfection efficiency to HSCs than PEI/ASO. The positively stained α-smooth muscle actin (α-SMA) is a marker of the activated HSCs.

Because targeted delivery of therapeutic agents to the HSCs in the liver requires the delivery system to meet two major requirements (it needs to be recognized by HSCs and, before reaching the liver, it can evade the phagocytosis of macrophages in the circulation), we performed another experiment to compare the transfection efficiency of RAP between to HSCs and to macrophages, by using a well-established HSC cell line HSC-T6 cell[15] and a macrophage cell line Raw 264.7. It is shown in Figure 4B that RAP transfected more HSC-T6 than Raw 264.7 cells; on the contrary, the PEI/ASO complex transfected more macrophages. The transfection performance of RAP to the two HSCs was high and consistent, as analyzed by flow cytometry for its transfection efficiency to primary HSCs (Figure 4C) and HSC-T6 cells (Figure 4D). Moreover, in the serum-containing media, transfecting the ASO against collagen I by RAP could significantly down-regulate the transcriptional level of collagen I expression in fibrotic HSCs (Figure 4E), which only slightly decreased in the PEI/ASO-transfected group (Figure 4F). The protein level of collagen in RAP treated cell was also significantly reduced (Figure 4G). These results together demonstrated that RAP has remarkable transfection effect for HSC and could facilitate the anticollagen I ASO interference in the activated fibrotic HSCs.

Influence of Albumin, RBP, and Retinol on the Transfection of RAP. In our strategy, the transfection of RAP to HSC should be mediated by the combination of RBP and the retinol motif on RAP. The albumin would help the particle to evade the phagocytosis of macrophages. To test this, we performed the transfection experiments to HSC-T6 cells in serum-free media. First, as shown in Figure 5A, PEI/ASO complex effectively transfected both cells, while albumin-associated RAP had low transfection efficiency to either HSCs or macrophages. Notably, the Albumin/RBP/RAP complex demonstrated remarkably high efficiency in transfecting the ASO into HSCs while delivering very few oligonucleotides to the macrophages. In comparison, free ASO could hardly transfect either macrophages or HSCs, while RAP exhibited moderate and low transfection efficiency to macrophages and HSCs, respectively. These findings validated our hypothesis that the specific receptors to RBP on HSCs could facilitate the RBP-bound complexes to enter these cells and albumin had the effect to prevent RAP to be captured by macrophages. Second, we performed a flow cytometry analysis to quantify the influence of albumin and RBP on the transfection of RAP to HSCs. Consistent with the above findings, with free ASO as control, addition of RBP into the medium had no influence on the PEI/ASO transfections but significantly increased the transfection efficiency of Albumin/RAP complexes in HSCs (Figure 5B). In the HSCs treated with RAP, we saw an increase in both the concentration of RBP in the media and the numbers of cells that were successfully transfected (Figure 5C), indicating that the transfection of the RAP into HSC was through the RBP-mediated phagocytosis. Next, we added free retinol into the media in order to competitively bind RBP before transfection. We found that the free retinol greatly compromised the transfection ability of Albumin/RBP/RAP complex, but had little influence on that of PEI/ASO complex. RAP – in serum-supplemented media—showed similar transfection efficiency to the

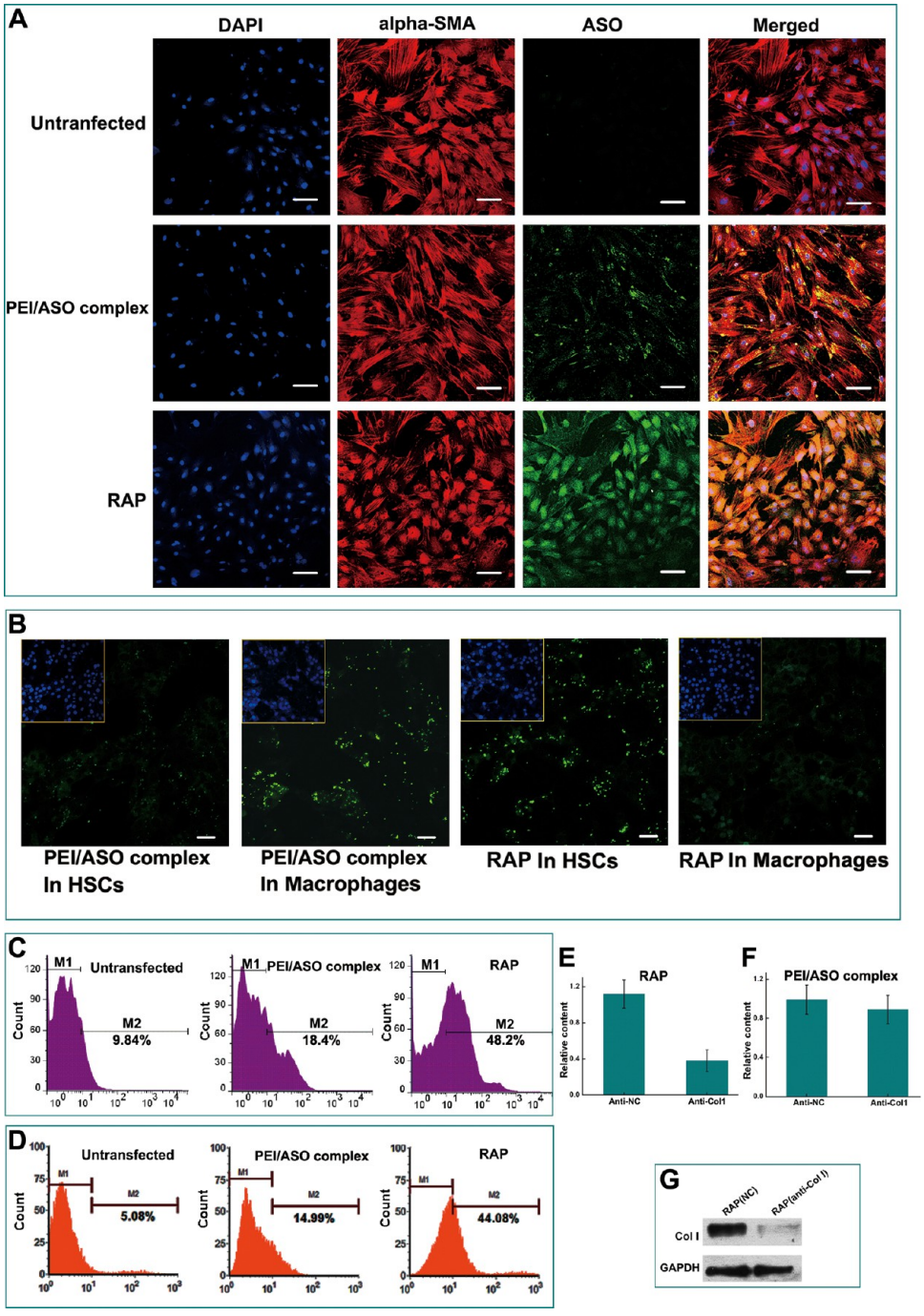

Figure 4. *In vitro* transfection effect of RAP. (A) Representative fluorescent photographs of primary mouse HSCs transfected with PEI/ASO complex or RAP in the media with 10% bovine serum for 12 h. The α-SMA was stained by rhodamine-labeled antibody to demonstrate the cells separated from fibrotic mouse liver were activated HSCs. The fluorescent ASO labeled by FAM was shown in green. DAPI stained nucleus indicated the cell number and position in the photographs. (B) Photographs of HSC-T6 cells and macrophages transfected with fluorescent-ASO by PEI/ASO complex or RAP in the media supplemented with 10% bovine serum for 12 h. Green fluorescence indicates cells with fluorescent ASO labeled by FAM, and the upper left square shows DAPI stained cell nucleus indicating the position of each cell in the picture. (C) The transfection efficiency of PEI/ASO complex and RAP to primary HSCs in the media with 10% bovine serum for 12 h, quantified by flow cytometry. (D) The transfection efficiency of PEI/ASO complex and RAP to HSC-T6 cells in the media with 10% bovine serum, quantified by flow cytometry. (E) The transcriptional level of collagen I in activated HSC-T6 cells transfected with anti-Col1 ASO by RAP. (F) The transcriptional level of collagen I in activated HSC-T6 cells transfected with anti-Col1 ASO by PEI/ASO complex. (G) Western blotting analysis of collagen I expressed by HSC-T6 cells transfected with anti-Col1 ASO by RAP in the presence of bovine serum. Intensity of the bands reflects relative abundance of individual proteins. GAPDH is the internal control of the test indicating the relative total protein contents in each sample. The fluorescent photographs were taken by confocal microscopy. Data in (E) and (F) are presented as means ± SD of three independent experiments. Images in (A), (B), (C), (D), and (G) were representative of three independent results. Scale bar in all microphotographs: 50 μm.

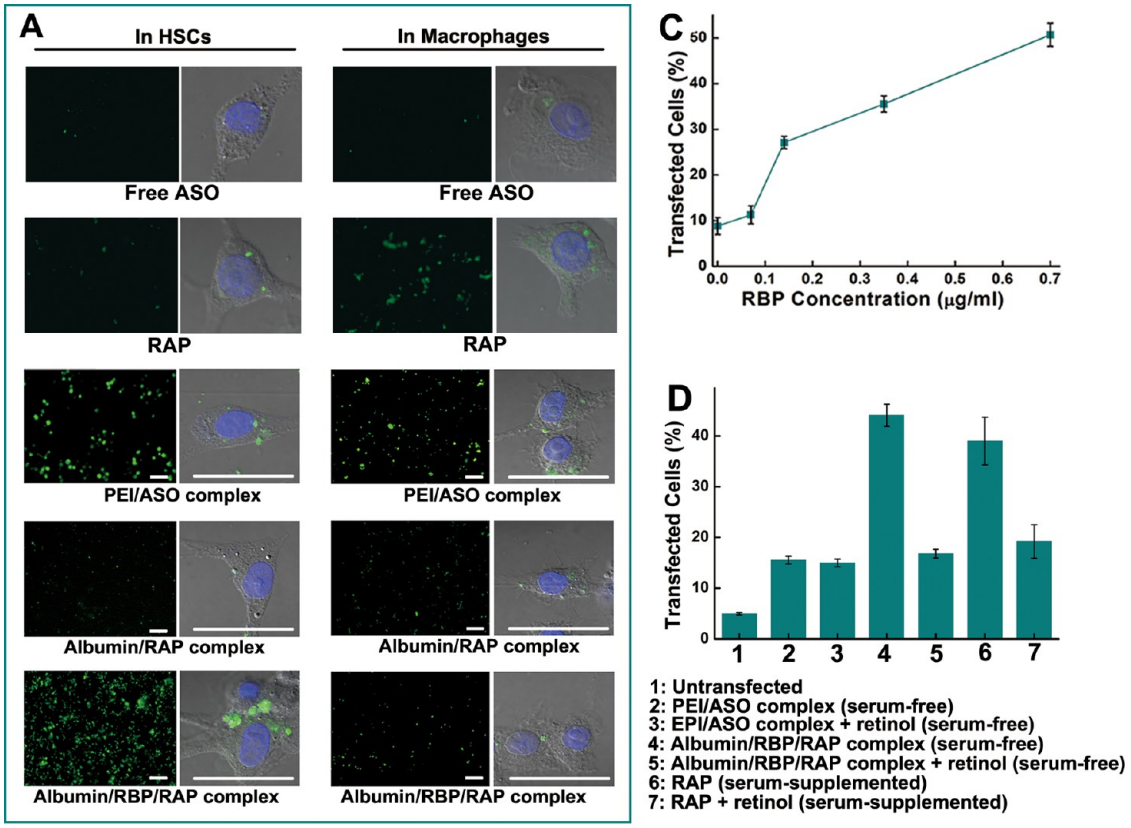

Figure 5. The influence of albumin, RBP and retinol on the transfection effect of RAP. (A) Fluorescent microscopy photographs of HSC-T6 cells and macrophages transfected by Free ASO, RAP, PEI/ASO complex, Albumin/RAP complex and Albumin/RBP/RAP complex in serum-free media; green fluorescence indicates cells transfected with the fluorescent ASO for 12 h. (B) Quantitative analysis of the transfection efficiency of Albumin/RBP/RAP complex in serum-free media for 12 h by flow cytometry, with free ASO, PEI/ASO complex, PEI/ASO complex with RBP and Albumin/RAP complex as the controls. (C) Transfection efficiency of RAP to HSC-T6 cells for 12 h cultured in the serum-free media in the presence of various concentrations of RBP (0−0.7 μg/mL), determined by flow cytometry. (D) The transfection efficiency of PEI/ASO complex or Albumin/RBP/RAP complex to HSC-T6 cells cultured in the serum-free or serum-supplemented media for 12 h with or without retinol (5 mg/mL). (E) The transfection efficiency of RAP to HSC-T6 cells in the media containing 10% serum for 12 h in the presence of RBP antibody, quantified by flow cytometry and with free ASO and PEI/ASO complex as the control. Data in (C) and (D) are presented as means ± SD of three independent experiments. Images in (A), (B), and (E) were representative of three independent results. Scale bar in all microphotographs: 50 μm.

Albumin/RBP/RAP complex in serum-free media, and addition of retinol to the serum-supplemented media also greatly inhibited the transfection of RAP (Figure 5D). Additionally, to further verify the role of RBP in the transfection process of RAP to HSCs, we employed an antibody to RBP to neutralize the RBP in serum-containing media. As shown in Figure 5E, the transfection of RAP to HSC-T6 cell in the serum-containing media was efficiently blocked while the antibody had little influence on the transfection of PEI/ASO complex. These outcomes confirmed the pivotal role of RBP for RAP transfection.

But why did PEI/ASO complex and RAP exhibit distinct transfection efficiency to macrophages, when both of them had albumin as the most abundant protein in their corona components? To address this

question, we tested the effect of extra albumin, added to the formed PEI/ASO complex and RAP, on the transfection efficiency of these two complexes. In the serum-free macrophage culture, albumin did not significantly change the transfection efficiency of PEI/ASO complex, but almost completely disabled RAP to transfect the cells (Supporting Information Figure S2). Such difference might be caused by the different modes of association between albumin and the two nanocomplexes. In contrast to PEI/ASO complex, RAP had a hydrophobic surface and bound albumin largely through a hydrophobic interaction, which helped albumin maintain its native conformation in the body.

Biodistribution and Cellular Location of the Intravenously Injected RAP. RAP injected intravenously was expected to be covered by a layer of protein corona from the plasma. In our design, the retinol block of RAP could recruit RBP, which would mediate the targeting of these particles to HSCs in the liver (Figure 6A).

In the liver fibrosis mouse model, we examined the *in vivo* distribution of the ASO-laden RAP, in which the ASO was labeled with rhodamine for tracing and quantification. Naked ASO was set as control. We found that 6 h after the injection *via* tail vein, both the naked ASO and RAP were mainly accumulated in the liver, but RAP-delivered ASO had much higher concentration there (Figure 6B). In other organs, the concentration of ASO, either delivered by RAP or naked, was found to be similar. In addition, a time-course change of the naked ASO and RAP-delivered ASO in the blood and in the liver tissue was determined. RAP-delivered ASO had longer circulating time than naked ASO (Figure 6C), which was important for the protein corona on RAP to evolve into an RBP-enriched form. Moreover, the RAP-delivered ASO was retained in the liver for a longer time than ASO, possibly because the carrier protected ASO from degradation in the body fluid (Figure 6D).

The ultimate target of RAP in liver is HSCs. We further determined the cellular localization of the ASO in the mouse liver, by using a fluorescent ASO (FAM-labeled ASO). The liver tissues were sectioned and analyzed by laser confocal microscopy, because we found that both the naked and RAP-delivered ASO were mostly located in the nonparenchymal cells around the hepatic sinusoids. In these areas, the main cells are macrophages, endothelial cells and HSCs. So we stained the three kinds of cells using an F4/80 antibody for macrophages, a CD31 antibody for endothelial cells, and an α-SMA antibody for HSCs. In the confocal photographs, fluorescent ASO was shown in green and the markers of the three cells were stained in red. The cell nucleus was counter-stained in blue with DAPI (Figure 6E, Supporting Information Figure S3). In the RAP group, ASO (green) was found to merge with HSCs (red) to generate strong yellow signals, indicating that most ASO molecules were located in HSCs. However, naked ASO was found mainly in the endothelial cells and macrophages. Additionally, in RAP group, a small fraction of labeled ASO was distributed in the parenchymal cells (Figure 6E, Supporting Information Figure S3). This was not found in the naked ASO group, suggesting that RAP could evade the filtration of the reticuloendothelial system and reach the parenchymal cells. Taken together, these results clearly demonstrated that, when administrated *via* the circulation, RAP could target, and deliver ASO into HSCs *in vivo*. Test of PEI/ASO complex in this experiment could not be completed because intravenous injection of PEI/ASO complex caused instantaneous death of the animals even at very low doses (<0.5 mg/kg body weight) (Supporting Information Figure S1).

Antifibrosis Activity of RAP. The ultimate purpose of targeted delivery of ASO to HSCs was to treat liver fibrosis. After entering HSCs, the ASO was expected to be released from the complex and suppress the expression of pathological genes and prevent the development of liver fibrosis (Figure 7A). We set up a CCl_4-induced liver fibrosis in mice to evaluate the therapeutic performance of the ASO (anti-Col1), which was designed against collagen I, with a scrambled ASO (anti-NC) as control. The entire course of treatment was illustrated in Figure 7A.

We found that the treatment significantly lowered the content of hydroxyproline, one of the main constituents of collagen and thus one important marker for pathological fibrosis (Figure 7B). Collagen I, the direct target of the ASO, was found to be successfully decreased by RAP-delivered ASO in the fibrotic liver at both the transcriptional level (Figure 7C), as determined by quantitative RT-PCR, and the protein level, as evaluated by Western blotting (Figure 7D) and quantification (Figure 7E). In concert, histological analysis of the mice liver tissue sections suggested that RAP-delivered ASO significantly reduced the number of highly proliferative HSCs (hematoxylin and eosin (H&E) staining, Figure 7F,G) and collagen deposition (Sirius Red staining, Figure 7F,H). In all tests above, the RAP group significantly improved the therapeutic performance of the ASO, in comparison with the naked ASO group ($P < 0.05$). Treatment with RAP achieved successful inhibition of the development of hepatic fibrosis. To further validate the efficacy of RAP, we tested it in the bile duct ligation (BDL) mice, another mouse model for liver fibrosis. The data shown in Supporting Information Figure S4 were in consistent with the results obtained from CCl_4 animal model.

Additionally, we performed a stringent therapeutic test of RAP on CCl_4 fibrosis model. The fibrosis animal models received the RAP treatment 4 weeks after the models were given CCl_4 for liver fibrosis induction. RAP was given to the animals once a week for 3 weeks along with the 2 injections of CCl_4 every week. After the animals were sacrificed, the hydroxyproline content and collagen I mRNA level in the liver tissues were

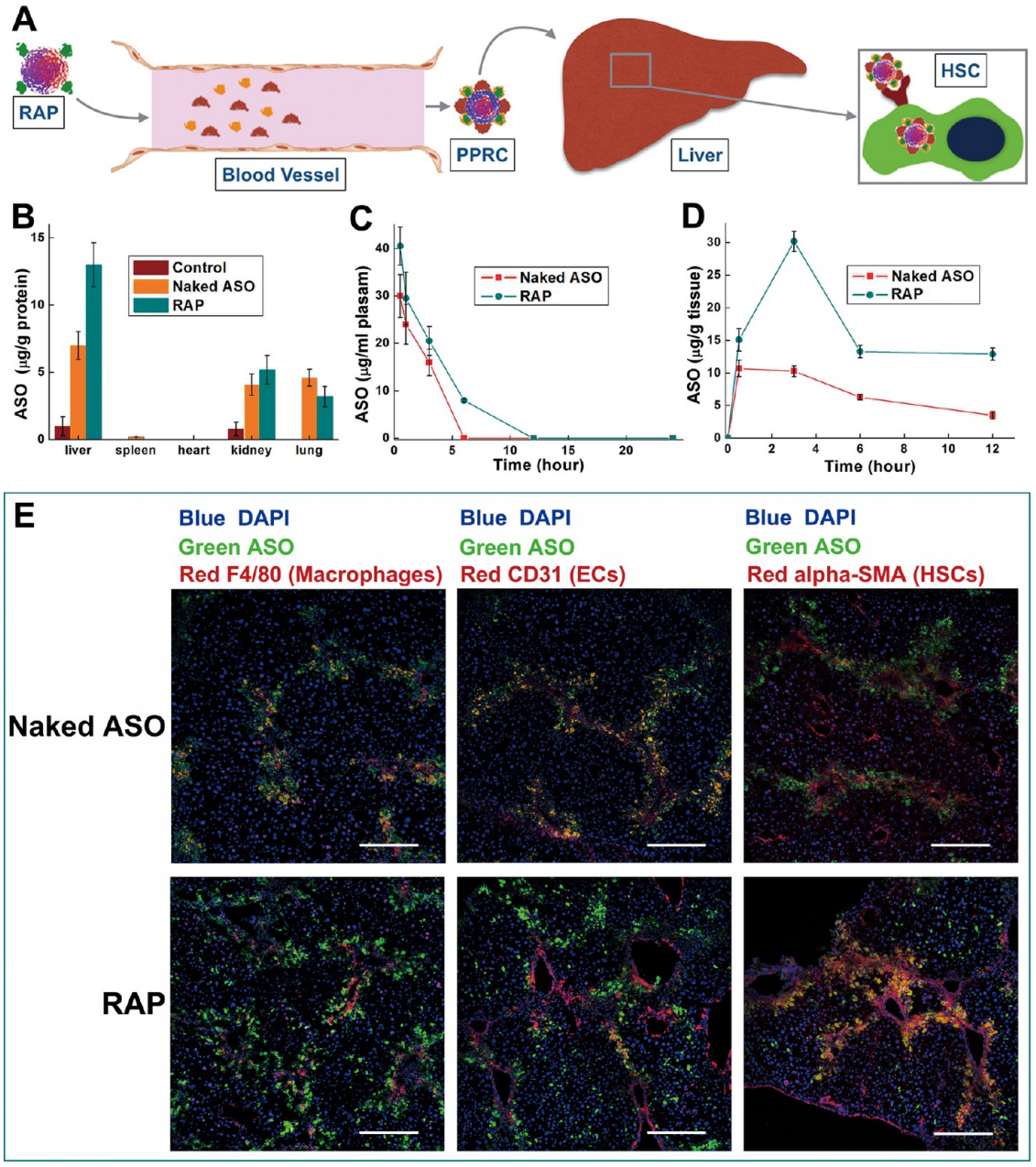

Figure 6. Biodistribution and cellular location of the intravenously injected RAP. (A) Schematic diagram showing the theoretical fate of RAP administered intravenously. (B) ASO (naked or delivered by RAP) distribution in different organs, quantified for fluorescence intensity. (C and D) Time-dependent ASO (naked or delivered by RAP) concentrations in (C) the blood and (D) the liver, quantified for fluorescence intensity. (E) Confocal microscopic observations of the cellular distribution of the transfected ASO (naked or delivered by RAP) in the liver. The liver tissue was sectioned and immunofluorescent stained by an α-SMA antibody (red) for HSCs, an F4/80 antibody for macrophages (red), a CD31 antibody for endothelial cells (red), and DAPI for cell nucleus (blue). The fluorescent ASO was shown in green. Co-localization was determined where the green and red fluorescence perfectly merged into yellow signals. The fluorescent photographs were taken by confocal microscopy. Scale bar: 100 μm. Representative images of three independent results were presented. Data are presented as means ± SD of three independent results (n = 6 in each group).

examined. Data shown in Supporting Information Figure S5 suggested that although the hydroxyproline level was higher than that in Figure 7B after RAP treatment (Supporting Information Figure S5A), the mRNA level of collagen I was significantly down-regulated by the treatment (Supporting Information Figure S5B). The data indicated that, although the collagen I accumulation in mouse liver during the 4-week model induction was not inhibited very well by RAP treatment, the collagen I expression in the liver was immediately blocked by RAP delivered anticollagen I ASO.

DISCUSSION

Targeted delivery of drugs to specific sites in the body requires rational design of the carrier system, based upon thorough understanding of the interaction

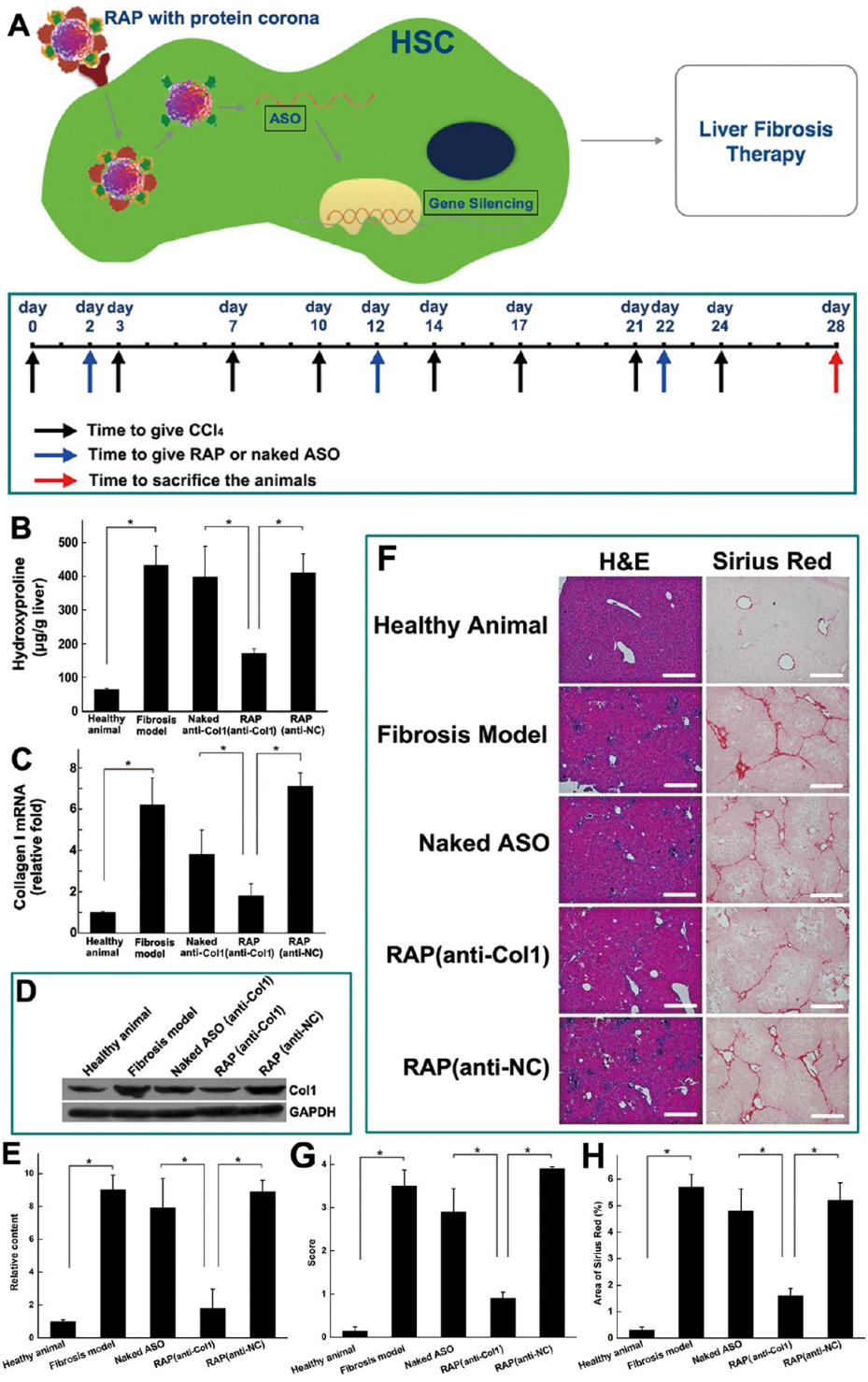

Figure 7. ASO against collagen I delivered by RAP ameliorated murine liver fibrosis. (A) Schematic diagram showing the induction of the murine hepatic fibrosis by CCl_4, and administration of the naked ASO or RAP (RcP/ASO complex). The ASO (anti-Col1) was designed to inhibit the expression of collagen I, and the control group (anti-NC) was a scrambled noncoding DNA fragment with the same length and GC contents as anti-Col1. Naked anti-Col1 was set as another control to verify the efficacy of the delivery carriers. (B) The hydroxyproline content in mice liver. (C) The collagen I mRNA in the liver of animals with different treatments determined by qRT-PCR. (D) The levels of the collagen I protein in the liver of animals following different treatments, determined by Western blotting. The Western blot results represented one of three independent cohorts. (E) Densitometric quantification of the Western blotting results of all the animals in each group. (F) Representative of H&E and Sirius Red staining of liver tissue sections. The blue area in H&E staining indicates the proliferating HSCs, and the red areas in Sirius red staining sections indicate the collagen deposition in the fibrotic liver tissues. (G) The score of H&E staining sections of all the animals in each group. (H) Semiquantitative analysis of the area of Sirius Red staining sections of all the animals in each group. Scale bar, 100 μm. Data was given as means $\pm$ SD of three independent experiments ($n \geq 6$ in each group). *$P < 0.05$.

between the carriers and the biomolecules *in vivo*. Increasing evidence suggest that once a nanosized particle enters the circulation, proteins in the blood plasma rapidly form a layer of "corona" on its surface, which endows the drug carrier with new "biological identity" in the body.[16] The type and amount of the corona proteins would dictate the transportation routes and final destination of the vehicle.[17] As such, harnessing the power of the corona proteins holds a crucial position, whereas largely underestimated, in the design of strategies for targeted drug delivery *in vivo*. In our study, we demonstrated a drug delivery system that recruited two plasma proteins, albumin and RBP, into the corona on the vehicle surface. These two proteins exhibited significant but different functions to direct the vehicle to the specific hepatic stellate cell populations, and thereby enhanced the therapeutic efficacy of the system against liver fibrosis.

Albumin was recruited in the corona on the RcP surface to play two essential roles. First, albumin is a versatile transporter for a wide range of nutrient molecules in the body;[18,19] here, it acted in its native role to direct the vehicle to the liver. Second, albumin has the unique capability of going through the filtration system in the body without being phagocytized;[20] in the present design, albumin prevented the delivered ASO vehicle from being filtered by the reticuloendothelial system *in vivo*. Albumin was recruited to the vehicle surface in several mechanisms. First, albumin is the most abundant protein in the plasma and has a high chance of adsorption onto the surface of a foreign particle entering the circulation. Second, albumin is negatively charged and the RcP positively charged, facilitating the electrostatic binding between them. Third, in physiological conditions, retinol can also bind albumin,[21] making the interaction between albumin and the vehicle more specific. As retinol is a hydrophobic molecule on the vehicle surface, its binding with albumin would enhance the dispersion of the vehicle and avoid the recognition of the delivery system by phagocytes. Indeed, we demonstrated that the recruitment of albumin onto the particles of RcP/ASO significantly decreased the phagocytosis by macrophages both *in vitro* and *in vivo*. In contrast, the unmodified PEI/ASO particles, despite their ability to recruit albumin, were largely captured by macrophages when tested *in vitro*. Such findings further highlight the necessity of the retinol modification.

But why did these two complexes, retinol-conjugated PEI/ASO and unconjugated PEI/ASO, have eventually different fates *in vivo*? We postulate that albumin bound to the complexes in different scenarios. The unmodified PEI is a hydrophilic molecule, binding albumin *via* the electrostatic force and hydrogen bonds. As a result, the hydrophobic region of albumin is exposed. However, in the case of retinol conjugated PEI, the particles bind albumin mainly *via* the hydrophobic interactions between the retinol motif on the particle and the hydrophobic domains of albumin. The latter interaction may help to maintain the "correct" configuration of albumin and thus native function as a transporter for retinol. Also, the negative charge of albumin is essential to its function.[22] The unmodified PEI might be too positive in charge and disrupt the native state of albumin. To validate these interpretations, we need in future work more evidence, both theoretical and empirical, to uncover the precise roles of albumin and the detailed mechanism of how it is recruited to the particle.

The second protein we designed to recruit in the corona was RBP. The role of RBP in our delivery system is crucial—it directed the drugs to the specific cell population, HSCs. In human body, up to 90% of total body retinols are stored in the liver, and 80% of these liver retinols are in HSCs.[23] As RBP is the sole transporter for retinol in the circulation, HSCs can efficiently take RBP-bound retinol from the blood.[24,25] It was demonstrated in a previous study that retinol-conjugated liposomes could be preferentially taken up by HSCs.[26] However, HSCs do not take RBP, the carrier itself, without retinol. Again, retinol conjugation in our design played essential roles, not only in recruiting RBPs to the vehicle surface, but also in functionalizing these transporter proteins. Activated by the retinol on the vehicle, RBPs efficiently directed the vehicle complex into HSCs.

It should be noted that the formation of corona is highly dynamic,[27] and is influenced by various factors such as surface chemistry, physiological conditions, and ligand affinity.[28,29] Although the most abundant protein may initially be presented in the protein corona on the particle, they may be replaced by other proteins, which are less abundant but have higher affinity for specific ligands on the vehicle surface. This process is known as "corona evolving".[30,31] In our system, RBP, despite its relatively lower abundance in the plasma, was enriched in corona because of its specific affinity for the retinol ligand. The two corona proteins we harnessed in this study represent different ways of corona formation and exhibited different functions; in collaboration, they protect the delivery complex and direct the therapeutic agents to the target cells in the body.

Besides their different targeting properties, the two vehicle complexes, RAP and PEI/ASO, exhibited completely different behavior, including their *in vitro* and *in vivo* toxicity and pro-coagulant activity. We attributed these differences to the large discrepancy in the compositions of their protein coronas. The significant increase in the amount of RBP was due to the specific recognition and combination between retinol molecules and RBP. The other differences in protein composition of the corona may be mainly caused by the different physiochemical properties in the surfaces

of the two particles. The PEI/ASO complex had a highly hydrophilic, positively charged surface while the RAP one had a more hydrophobic surface because of the introduction of retinol molecules. The difference was obvious in their aqueous solution. The solution of RAP appeared to be emulsion while PEI/ASO a clear solution. These results indicated that introducing one molecule to the composition of a nanoparticle could radically change the protein corona. Furthermore, an important and advantageous feature of the RAPs was their prolonged circulating time, which we attribute to the proper way in which the albumin bound the particle in the protein corona. This feature allows RBP, which is relatively low in the plasma content, to be enriched in the corona formed on the vehicle surface.

Hepatic fibrosis represents a progressive, pathological change in the liver. Inhibition of hepatic fibrosis would effectively prevent its development into irreversible cirrhosis and malignant liver cancer. The activated HSCs are the principle target cells for the treatment of hepatic fibrosis;[32] however, current therapies have found it very difficult to target these cells, because they merely constitute less than 10% of total liver cells,[33] and are located perisinusoidally behind the filtration system of endothelium and macrophages. To overcome this challenge, we exploited the native transportation proteins that can reach such specific cell population, and recruited them as corona proteins that showed high specificity in directing the therapeutic nucleic acids to the target cells. Our therapeutic strategy of delivering antisense oligonucleotides to suppress the expression of type I collagen has proven efficacious in inhibiting the development of hepatic fibrosis. In general, tissue fibrosis is one of the biggest challenges to modern medicine, and its pathogenic mechanisms are extremely complex.[34] Therefore, to target the downstream factors would be relatively safer and more efficient than to target the upstream ones. Specifically, to reduce the production and deposition of collagen I, which is the final pathological factor in hepatic fibrosis, in the liver tissue represents one of the most direct therapeutic strategies for this disease.[35] In this study, we designed the ASO to target the overexpressed type I collagen, and demonstrated that, by using the HSC targeted delivery system, these ASO efficiently suppressed the expression of type I collagen, and ameliorated the development of hepatic fibrosis in the murine model.

CONCLUSION

In conclusion, our present study demonstrates that control and harnessing of the corona protein formed on the drug vehicles can be a new strategy for the design of smart vehicles for targeted delivery. Introduction of retinol specifically recruited RBP in the corona that successfully directed the drug-laden particles into the HSCs in the liver, and meanwhile changed the hydrophicility of the vehicles and thereby helped them escape the filtration by the immune cells in the circulation. Such a simple, direct and unsophisticated modification efficiently delivered the antifibrosis ASO to the specific cell population in the site of disease, leading to satisfactory therapeutic performance. In concert with other recent studies aimed at analyzing the formation of corona *in vivo*, our investigation represents an innovative attempt to manipulate the formation of corona *in vivo* and to exploit the native functions of corona proteins for drug targeting in the body. We recommend this antisense delivery system be further trialed in more disease models of tissue fibrosis, for systematic evaluation of its therapeutic potential for clinical applications.

MATERIALS AND METHODS

Reagents and Synthesis of Materials. The antisense oligodeoxynucleotide (ASO) against mouse collagen I mRNA with the sequence 5′-ACTGTCTTCTTGGCCATGCG-3′ was verified.[36] The mismatched ASO with the sequence 5′-CGCATGGCCAAGAAGACAGT-3′ was set as the control. The antisense oligodeoxynucleotides (ASOs) with full phosphorothioate linkage were synthesized by SBS Genetech Co., Ltd. (Shanghai, China). The recombinant mouse RBP (retinol binding protein 4) was purchased from Sino Biological, Inc. (Beijing, China). Dimethyl sulfoxide (DMSO), PEI, CDI and all the other reagents were obtained from Sigma (St. Louis, MO).

Retinol-c-PEI (RcP) was synthesized according to the following methods. Generally, Retinol was coupled to PEI (1.3 kDa) by an *N*,*N*′-carbonyldiimidazole (CDI) activation method according to the previous study.[37] In total, 1.0 mL of retinol (about 1.0 g) and 0.56 g of CDI were added to 20 mL of dehydrated dimethyl sulfoxide (DMSO). Following agitation using magnetic stirrer at 30 °C for 24 h, 4.32 g of PEI (1.3 kDa) was further added into the reaction mixture, and this stirred at 30 °C for 24 h. The resulting Retinol-c-PEI was dialyzed for 4 days against double distilled water and was lyophilized. The resulting RcP was determined by FT-IR spectra and NMR analysis. The ability of Retinol-c-PEI to bind DNA was determined by agarose gel electrophoresis. Retinol-c-PEI/DNA complexes were prepared by mixing 1 mg/mL Retinol-c-PEI solution (in saline, at room temperature for 2 h) with 100 bp fish sperm DNA solution of different concentrations (in saline) in order to obtain complexes with different ratios of $M_{\text{Retinol-c-PEI}}/M_{\text{DNA}}$. Then the complexes were examined by gel electrophoresis (0.8% agarose in TAE buffer). PEI was used as the control.

Characterization of the Particles. The morphology of PEI/ASO complex, RAP, Albumin/RAP complex, RBP/RAP complex and serum-incubated RAP was determined by a transmission electron microscope (JEM-200CX, Jeol, Tokyo, Japan). Particles incubated with different solutions and serum were separated and purified according to a published method.[38] Samples were diluted with distilled water and then loaded on Formvar-coated copper grids, dried at room temperature, and stained with the aqueous solution of phosphomolybdic acid 2% (w/v). The intensity-average diameter and polydispersity index (PDI) of PEI/ASO complex, RAP, Albumin/RAP complex, RBP/RAP complex and serum-incubated RAP were measured at the concentration of 1−2 mg/mL, using a 90plus Particle Sizer (Brookhaven Instruments, NY). Zeta-potential measurements were performed for 1/10 dilutions of the dispersions in

phosphate-buffered saline (pH = 7.4), based on the electrophoretic mobility of the particles in a clear, disposable capillary electrophoresis cell. The association between proteins and PEI, RcP or different complexes was determined by the native PAGE. Proteins combined with PEI or the particles would be retarded in the process of electrophoresis. The proteins harvested from the corona on PEI/ASO complex or RAP formed in serum were analyzed by SDS-PAGE and Coomassie brilliant blue staining.

Sample Preparation for LC−MS Analysis. The nanoparticle−protein complexes were lysed with lysis buffer. Proteins eluted from nanoparticles were desalted (Zeba Spin Desalting Columns) and quantified; 100 μg total protein was reduced by adding 1 M DTT (60 °C, 1 h), and free cysteines were alkylated with 1 M iodoacetamide (room temperature, 10 min in the dark). The alkylated proteins were centrifuged in the 10K ultrafiltration tube (12 000 rpm, 20 min, 4 °C), and the proteins were retained in the 10K ultrafiltration tube. The proteins were further washed three times with 100 mM TEAB buffer (12000 rpm, 20 min, 4 °C each time). The protein was first examined by a SDS-PAGE electrophoresis. Then a 2 μg amount of porcine sequencing grade trypsin was added in to the ultrafiltration tube, and the samples were incubated overnight at 37 °C. After digestion, the resulting peptides were collected into a new vial by centrifugation (12 000 rpm, 20 min, 4 °C). To remove any potential biomaterials in the samples before LC−MS analysis, the resulting peptides were further enriched by C18 reversed-phase columns (Macrospin Column Silica C18), and the samples were set to LC−MS analysis with AB Sciex Triple ToF 5600$^+$ (AB SCIEX, MA). Samples were analyzed in three technical replicates.

Cell Culture. For the isolation of primary activated HSCs from fibrotic livers, the activated HSCs could be isolated by discontinuous density gradient centrifugation according to published protocols.[39,40] The mouse liver was perfused from the left ventricle of the heart with a heparin sodium buffer, while the inferior vena cava was used as the outflow until the liver became pale. The perfusion was continued with collagenase (Roche Applied Science; 3 mg/mL) and Pronase (Sigma; 3 mg/mL) buffer. The liver was carefully removed and dissociated in digestion medium II (0.5 mg/mL collagenase and Pronase, 0.2 mg/mL DNase I) for further digestion. Afterward, the liver cell suspension was filtered through gauze (100 μm) and centrifuged for 5 min at 50 μg at 4 °C to obtain the parenchyma cells. The nonparenchyma cells were collected from the 50 μg supernatant and washed twice before density gradient centrifugation. The purity of isolated activated HSCs was determined by α-SMA fluorescence staining; the purity exceeded 90%.

HSC-T6 cells and Raw 264.7 were purchased from Institute of Biochemistry and Cell Biology (SIBS, Shanghai, China). HSC-T6 cells, Raw 264.7 cells or isolated primary HSCs were routinely cultured in Dulbecco's Modified Eagle's medium (DMEM; Gibco, MA) containing 10% FBS (Invitrogen) at 37 °C with 5% CO_2 and humidity. For serum free culture, HSC-T6 cells or Raw 264.7 cells were cultured in a serum free media (Opti-MEM, Gibco, MA).

Cell Survival Assay. Approximately, 10 000 cells were plated into each well of 96-well flat-bottomed microtiter plates. Twelve hours later, medium containing different concentrations of PEI (1.3 or 25 kDa)/ASO complex, or RAP was added into the cells. After 24 h incubation, 10 μL of CCK-8 was introduced into each well and the mixture was incubated for 2 h. The plates were spectrophotometrically analyzed with microplate reader (Infinite M1000 PRO, Tecan, Männedorf, Schweiz) at 450 nm.

Cell Transfection. Primary mouse HSCs separated from the fibrotic livers of the CCl_4 liver fibrosis animal models, HSC-T6 and Raw 246.7 cells were used in the transfection experiments. Cells were cultured in 24 well plates to reach 70−80% confluence. The transfection efficacy was first examined in complete media. PEI/ASO complex or RAP containing 1 μg fluorescent ASO was added into the media for 12 h, and analyzed by confocal microscopy and flow cytometry. To investigate the influence of albumin, RBP and retinol, the experiments were conducted in the serum-free media. RcP/ASO complex was mixed with albumin in the absence or presence of RBP, to form Albumin/RcP/ASO complex or Albumin/RBP/RcP/ASO complex, respectively; PEI/ASO complex and Albumin/PEI/ASO were also tested. Cells were cultured in 24 well plates to reach 70−80% confluence, and the complete medium (Gibco DMEM containing 10% fetal bovine serum) was replaced by the serum free media. Then different complexes containing 1 μg fluorescent ASO were added into the cells for 12 h before further analysis, separately. The transfected cells were stained with DAPI for the nucleus and examined by a confocal microscopy (C2 plus, Nikon, Japan). To clarify the role of RBP in HSC-T6 cell transfection, RBP was further added into PEI/ASO complex and Albumin/RcP/ASO complex transfections in HSC-T6 cells. The transfection efficiency was monitored by flow cytometry analysis (Facscalibur, BD, MA). Further, the Albumin/RcP/ASO complex transfections (for 12 h) in HSC-T6 cells were determined in the serum free media containing 0−0.7 μg/mL RBP. For the blocking assay, before the Albumin/RBP/RcP/ASO transfections, 5 mg of free retinol was added into the 0.3 mL culture media, and then the transfection efficacy (cells were transfected for 12 h) was determined. Additionally, in serum containing media, the transfection of RAP was conducted with or without the pretreatment with a RBP blocking antibody (goat polyclonal to RBP4, Abcam, MA), at a concentration of 20 μg/mL for 1 h. The detection parameters, including the laser power value and photomultiplier high voltage power supply (PMT HV), for the confocal assay and the detection voltage flow cytometry analysis, should be determined by the negative control. No positive signals should be detected for cells without treatment. The detection parameters were the same within one experiment and variation should be less than 5% among repeated assays.

Tissue-Distribution and Cellular Localization of ASO Delivered by RAP. To determine the tissue distribution, the naked fluorescent ASO (rhodamine conjugated ASO) and RAP (containing the fluorescent ASO) solutions were injected into mice that were given CCl_4 for liver fibrosis induction for 4 weeks *via* tail vein at an ASO dose of 1.5 mg/kg body weight, separately. Animals were sacrificed at indicated time points, and different organs were harvested from the animals. ASO in the tissues was extracted and quantified by examining the fluorescence intensity at 556 nm according to the previous study.[41] Briefly, ASO in different tissue homogenates were extracted using a phenol−chloroform method and examined for their fluorescent intensity. Their quantity was calculated based on a standard curve that was made by compare different amount fluorescent ASO to their fluorescent intensity in the same solvent. The final content of ASO in each organ was further calculated according to the extraction rates. To obtain the extraction rate, a certain amount of ASO was added into the homogenate made of the same organ from a clean mouse with no treatments and extracted by using the same extraction protocol. The extraction rate was calculated by comparing the amount of extracted ASO and the initial ASO added into the homogenate. The time dependent quantification in serum and liver tissue used the same protocol.

To determine the cellular location in the liver, a FAM (6-carboxyfluorescein) conjugated ASO was used as the fluorescent ASO. Liver tissues were harvested and frozen-sectioned 4 h after RAP administration *via* the tail vein. The sections were stained with a rabbit anti-mouse α-SMA antibody (Abcam, MA) for HSCs, a rabbit anti-mouse F4/80 antibody (Abcam, MA) for macrophages or a rabbit anti-mouse CD 31 antibody (Abcam, MA) for endothelial cells at 4 °C overnight. The secondary antibody, rhodamine-labeled goat anti-rabbit, was applied at 37 °C for 45 min, followed by the staining of nuclei with 4,6-diamidino-2-phenylindole (DAPI) (Sigma-Aldrich, MO). Frozen sections were imaged by a confocal microscope (C2 plus, Nikon, Japan). In the photographs, the fluorescent ASO was shown in green; the α-SMA, F4/80, and CD31 stained with different antibodies were shown in red fluorescence. The confocal microscope could precisely detect the location of each cell. So, if the green fluorescence and the red fluorescence came from the same cell, the two kinds of fluorescence would merge into a new yellow color in the image; otherwise, the red and green would be separated or just overlapp each other and generate no yellow color.

Animal Treatments. Male ICR mice (20 ± 2 g) of the same ground were obtained from the Animal Centre of Yangzhou University (Yangzhou, China). For generating CCl_4-induced liver

fibrosis, mice were randomly divided (each group contained at least 6 mice) with free access to water and laboratory chow. Mice received intraperitoneal (ip) injections of carbon tetrachloride (CCl_4 in oil, 1:3, 4 μL/g body weight) twice weekly for 4 weeks, whereas the control group received oil intraperitoneally. For the RAP treatment groups, a single dose of 100 μL of the naked ASO (5 μg/g body weight per mouse) or the RAP (100 μg/g body weight RAP which contains 5 μg/g ASO per mouse) was administered through the tail vein every 10 days. Mice were sacrificed at the indicated time points. The therapeutic test of RAP was performed on this animal model 4 weeks after the model was set up as above-mentioned, and the RAP was given once each week for 3 weeks alone with the twice a week of CCl_4 administration.

The BDL liver fibrosis model was generated according to a reported method.[42] Briefly, mice were anesthetized with an ip injection of ketamine (80 mg/kg) and xylazine (10 mg/kg). After midline laparotomy, the common bile duct was ligated 3 times with 6-0 silk and transected between the 2 most distal ligations. Sham operation was performed similarly except that the bile duct was not ligated or transected. RAP treatment was given 2 days after the BDL operation; the animals were injected RAP (100 μg/g body weight RAP which contains 5 μg/g ASO per mouse) *via* tail vein once a week for 3 weeks before they were sacrificed.

All experiments were conducted according to the use and care guidelines for the experimental animals from Jiangsu Province, China.

mRNA Quantification. Total RNA was extracted from tissues, and complementary DNA was synthesized. The transcript levels were detected *via* real-time reverse transcription polymerase chain reaction (qRT-PCR) on a real-time PCR system (ABI 7500, Life technologies, CA). Individual gene expression was normalized to β-actin mRNA. Primers used are listed as follows: *Col1-F:* TCC GGC TCC TGC TCC TCT TAG; *Col1-R:* AGG CCA TTG TGT ATG CAG CTG AC, and *beta-actin-F:* GAC CTC TAT GCC AAC ACA GTG C; *beta-actin-R:* GTA CTC CTG CTT GCT GAT CCA C.

Western Blotting and Modified Western Blotting. Tissue homogenate or protein coronas were separated and prepared. Proteins were separated by SDS-PAGE and transferred onto the polyvinylidine difluoride (PVDF) membranes. The membranes were blocked using skim milk and then incubated with diluted primary antibody at 4 °C with gentle shaking, overnight. After 5 times of washing, secondary HRP-conjugated antibody was incubated for 1 h at room temperature. After washing as before, positive signal was detected with fluorography using an enhanced chemiluminescence system (#7003, Cell Signaling Technology, MA).

To determine protein components in gel retardation, nanoparticles were mixed with serum and the mixture was separated by the native-PAGE (using a polyacrylamide gel without SDS). The proteins were then transferred on PVDF membrane and detected as above. It was noteworthy that all the buffers used in these experiments were free of SDS or other detergents

Histological Studies. Paraffin-embedded liver tissues in each group were stained with hematoxylin and eosin (H&E) and Sirius red staining and photographed at 100× magnification. Briefly, paraffin-embedded liver tissues were sectioned at 5 μm; after deparaffinization and hydration, sections were stained with an H&E staining Kit (Jiancheng Biotech, Nanjing, China) or in 0.1% (w/v) Sirius Red (Direct Red 80, Sigma-Aldrich, St. Louis, MO) in a saturated aqueous solution of picric acid for 1 h. Then, the slides were rinsed twice, each for 15 min in 0.01 N HCl to remove unbound dye. After dehydration, the slides were mounted.

Statistical Analysis. Data are presented as the mean ± SD. The differences between groups were analyzed by Mann–Whitney U test and, or if appropriate, by Kruskal–Wallis ANOVA test. Survival curves were analyzed by the Kaplan–Meyer log-rank test. $P < 0.05$ was considered as significance.

Conflict of Interest: The authors declare no competing financial interest.

Acknowledgment. This work was supported by the National Science Fund for Distinguished Young Scholars (81025019), the National Basic Research Program of China (2012CB517603), the National High Technology Research and Development Program of China (2014AA020707), the Program for New Century Excellent Talents in University (NCET-13-0272), the National Natural Science Foundation of China (31271013, 31170751, 31200695, 31400671, 51173076, 91129712 and 81102489), the Key Project of the Chinese Ministry of Education (108059), the Ph.D. Programs Foundation of the Ministry of Education of China (20100091120020, 20130091110037), Nanjing University State Key Laboratory of Pharmaceutical Biotechnology Open Grant (KF-GN-201409, 02ZZYJ-201307). C.W. acknowledges the funding support from the Science and Technology Development Fund, Macao (FDCT 048/2013/A2).

Supporting Information Available: The cytotoxicity, and physiological toxicity of RAP and PEI/ASO complex; the procoagulant activity of PEI and RcP; the transfection efficiency of PEI/ASO complex and RAP to macrophage with or without albumin in a serum-free culture of Raw 264.7 cell line; the cellular localization of fluorescent ASO in liver tissue from liver fibrosis model with separated fluorescent channels; the therapeutic effects of RAP to BDL liver fibrosis model; the hydroproxyproline content and collagen I expression level in the fibrotic livers of CCl_4 models with strict therapeutic RAP treatment. This material is available free of charge via the Internet at http://pubs.acs.org.

REFERENCES AND NOTES

1. Jain, K. K. Nanoparticles as Targeting Ligands. *Trends Biotechnol.* **2006**, *24*, 143–145.
2. Boyer, C.; Teo, J.; Phillips, P.; Erlich, R. B.; Sagnella, S.; Sharbeen, G.; Dwarte, T.; Duong, H. T.; Goldstein, D.; Davis, T.; *et al.* Effective Delivery of SiRNA into Cancer Cells and Tumors Using Well-Defined Biodegradable Cationic Star Polymers. *Mol. Pharmaceutics* **2013**, *10*, 2435–2444.
3. Whitehead, K. A.; Langer, R.; Anderson, D. G. Knocking Down Barriers: Advances in siRNA Delivery. *Nat. Rev. Drug Discovery* **2009**, *8*, 129–138.
4. Monopoli, M. P.; Aberg, C.; Salvati, A.; Dawson, K. A. Biomolecular Coronas Provide the Biological Identity of Nanosized Materials. *Nat. Nanotechnol.* **2012**, *7*, 779–786.
5. Mirshafiee, V.; Mahmoudi, M.; Lou, K.; Cheng, J.; Kraft, M. L. Protein Corona Significantly Reduces Active Targeting Yield. *Chem. Commun.* **2013**, *49*, 2557–2559.
6. Salvati, A.; Pitek, A. S.; Monopoli, M. P.; Prapainop, K.; Bombelli, F. B.; Hristov, D. R.; Kelly, P. M.; Åberg, C.; Mahon, E.; Dawson, K. A. Transferrin-Functionalized Nanoparticles Lose Their Targeting Capabilities When a Biomolecule Corona Adsorbs on the Surface. *Nat. Nanotechnol.* **2013**, *8*, 137–143.
7. Lesniak, A.; Salvati, A.; Santos-Martinez, M. J.; Radomski, M. W.; Dawson, K. A.; Åberg, C. Nanoparticle Adhesion to the Cell Membrane and Its Effect on Nanoparticle Uptake Efficiency. *J. Am. Chem. Soc.* **2013**, *135*, 1438–1444.
8. Prapainop, K.; Witter, D. P.; Wentworth, P., Jr. A Chemical Approach for Cell-Specific Targeting of Nanomaterials: Small-Molecule-Initiated Misfolding of Nanoparticle Corona Proteins. *J. Am. Chem. Soc.* **2012**, *134*, 4100–4103.
9. Pardridge, W. M. Transport of Protein-Bound Hormones into Tissues *in Vivo*. *Endocr. Rev.* **1981**, *2*, 103–123.
10. Fortuna, V. A.; Martucci, R. B.; Trugo, L. C.; Borojevic, R. Hepatic Stellate Cells Uptake of Retinol Associated with Retinol-Binding Protein or With Bovine Serum Albumin. *J. Cell Biochem.* **2003**, *90*, 792–805.
11. Mahley, R. W.; Rall, S. C., Jr. Apolipoprotein E: Far More Than a Lipid Transport Protein. *Annu. Rev. Genomics Hum. Genet.* **2000**, *1*, 507–537.
12. Quadro, L.; Blaner, W. S.; Salchow, D. J.; Vogel, S.; Piantedosi, R.; Gouras, P.; Freeman, S.; Cosma, M. P.; Colantuoni, V.; Gottesman, M. E. Impaired Retinal Function and Vitamin A Availability in Mice Lacking Retinol-Binding Protein. *EMBO J.* **1999**, *18*, 4633–4644.
13. Meir, K. S.; Leitersdorf, E. Atherosclerosis in the Apolipoprotein-E-Deficient Mouse: A Decade of Progress. *Arterioscler., Thromb., Vasc. Biol.* **2004**, *24*, 1006–1014.

14. Noy, N.; Xu, Z. J. Interactions of Retinol with Binding Proteins: Implications for the Mechanism of Uptake by Cells. *Biochemistry* **1990**, *29*, 3878–3883.
15. Vogel, S.; Piantedosi, R.; Frank, J.; Lalazar, A.; Rockey, D. C.; Friedman, S. L.; Blaner, W. S. An Immortalized Rat Liver Stellate Cell Line (HSC-T6): a New Cell Model for the Study of Retinoid Metabolism *in Vitro*. *J. Lipid Res.* **2000**, *41*, 882–893.
16. Aggarwal, P.; Hall, J. B.; McLeland, C. B.; Dobrovolskaia, M. A.; McNeil, S. E. Nanoparticle Interaction with Plasma Proteins As It Relates to Particle Biodistribution, Biocompatibility and Therapeutic Efficacy. *Adv. Drug Deliv Rev.* **2009**, *61*, 428–437.
17. Mahon, E.; Salvati, A.; Bombelli, F.; Lynch, I.; Dawson, K. A. Designing the Nanoparticle-Biomolecule Interface for "Targeting and Therapeutic Delivery". *J. Controlled Release* **2012**, *161*, 164–174.
18. Curry, S.; Mandelkow, H.; Brick, P.; Franks, N. Crystal Structure of Human Serum Albumin Complexed with Fatty Acid Reveals an Asymmetric Distribution of Binding Sites. *Nat. Struct. Biol.* **1998**, *5*, 827–835.
19. Nicholson, J. P.; Wolmarans, M. R.; Park, G. R. The Role of Albumin in Critical Illness. *Br. J. Anaesth.* **2000**, *85*, 599–610.
20. Kratz, F. Albumin as a Drug Carrier: Design of Prodrugs, Drug Conjugates and Nanoparticles. *J. Controlled Release* **2008**, *132*, 171–183.
21. Sivaprasadarao, A.; Findlay, J. B. The Mechanism of Uptake of Retinol by Plasma-Membrane Vesicles. *Biochem. J.* **1988**, *255*, 571–579.
22. Chonn, A.; Cullis, P. R.; Devine, D. V. The Role of Surface Charge in the Activation of the Classical and Alternative Pathways of Complement by Liposomes. *J. Immunol.* **1991**, *146*, 4234–4241.
23. Blaner, W. S.; O'Byrne, S. M.; Wongsiriroj, N.; Kluwe, J.; D'Ambrosio, D. M.; Jiang, H.; Schwabe, R. F.; Hillman, E. M.; Piantedosi, R.; Libien, J. Hepatic Stellate Cell Lipid Droplets: a Specialized Lipid Droplet for Retinoid Storage. *Biochim. Biophys. Acta* **2009**, *1791*, 467–473.
24. Blomhoff, R.; Berg, T.; Norum, K. R. Transfer of Retinol from Parenchymal to Stellate Cells in Liver Is Mediated by Retinol-Binding Protein. *Proc. Natl. Acad. Sci. U.S.A.* **1988**, *85*, 3455–3458.
25. Senoo, H.; Smeland, S.; Malaba, L.; Bjerknes, T.; Stang, E.; Roos, N.; Berg, T.; Norum, K. R.; Blomhoff, R. Transfer of Retinol-Binding Protein from HepG2 Human Hepatoma Cells to Cocultured Rat Stellate Cells. *Proc. Natl. Acad. Sci. U.S.A.* **1993**, *90*, 3616–3620.
26. Sato, Y.; Murase, K.; Kato, J.; Kobune, M.; Sato, T.; Kawano, Y.; Takimoto, R.; Takada, K.; Miyanishi, K.; Matsunaga, T.; *et al.* Resolution of Liver Cirrhosis Using Vitamin A-Coupled Liposomes To Deliver siRNA Against a Collagen-Specific Chaperone. *Nat. Biotechnol.* **2008**, *26*, 431–442.
27. Liu, W.; Rose, J.; Plantevin, S.; Auffan, M.; Bottero, J. Y.; Vidaud, C. Protein Corona Formation for Nanomaterials and Proteins of a Similar Size: Hard or Soft Corona? *Nanoscale* **2013**, *5*, 1658–1668.
28. Lundqvist, M.; Stigler, J.; Cedervall, T.; Berggård, T.; Flanagan, M. B.; Lynch, I.; Elia, G.; Dawson, K. The Evolution of the Protein Corona around Nanoparticles: A Test Study. *ACS Nano* **2011**, *5*, 7503–7509.
29. Walkey, C. D.; Olsen, J. B.; Guo, H.; Emili, A.; Chan, W. C. Nanoparticle Size and Surface Chemistry Determine Serum Protein Adsorption and Macrophage Uptake. *J. Am. Chem. Soc.* **2012**, *134*, 2139–2147.
30. Casals, E.; Pfaller, T.; Duschl, A.; Oostingh, G. J.; Puntes, V. Time Evolution of the Nanoparticle Protein Corona. *ACS Nano* **2010**, *4*, 3623–3632.
31. Milani, S.; Bombelli, F. B.; Pitek, A. S.; Dawson, K. A.; Rädler, J. Reversible *versus* Irreversible Binding of Transferrin to Polystyrene Nanoparticles: Soft and Hard Corona. *ACS Nano* **2012**, *6*, 2532–2541.
32. Friedman, S. L. Mechanisms of Hepatic Fibrogenesis. *Gastroenterology.* **2008**, *134*, 1655–1669.
33. Friedman, S. L. Seminars in Medicine of the Beth Israel Hospital, Boston. The Cellular Basis of Hepatic Fibrosis. Mechanisms and Treatment Strategies. *N. Engl. J. Med.* **1993**, *328*, 1828–1835.
34. Henderson, N. C.; Iredale, J. P. Liver Fibrosis: Cellular Mechanisms of Progression and Resolution. *Clin. Sci.* **2007**, *112*, 265–280.
35. Popov, Y.; Schuppan, D. Targeting Liver Fibrosis: Strategies for Development and Validation of Antifibrotic Therapies. *Hepatology* **2009**, *50*, 1294–1306.
36. Yan, Z.; Chen, M.; Perucho, M.; Friedman, E. Oncogenic Ki-ras But Not Oncogenic Ha-Ras Blocks Integrin Beta1-Chain Maturation in Colon Epithelial Cells. *J. Biol. Chem.* **1997**, *272*, 30928–30936.
37. Dong, L.; Xia, S.; Chen, H.; Chen, J.; Zhang, J. Spleen-Specific Suppression of TNF-alpha by Cationic Hydrogel-Delivered Antisense Nucleotides for the Prevention of Arthritis in Animal Models. *Biomaterials* **2009**, *30*, 4416–4426.
38. Tenzer, S.; Docter, D.; Kuharev, J.; Musyanovych, A.; Fetz, V.; Hecht, R.; Schlenk, F.; Fischer, D.; Kiouptsi, K.; Reinhardt, C.; *et al.* Rapid Formation of Plasma Protein Corona Critically Affects Nanoparticle Pathophysiology. *Nat. Nanotechnol.* **2013**, *8*, 772–781.
39. Bataller, R.; Sancho-Bru, P.; Ginès, P.; Lora, J. M.; Al-Garawi, A.; Solé, M.; Colmenero, J.; Nicolás, J. M.; Jiménez, W.; Weich, N.; *et al.* Activated Human Hepatic Stellate Cells Express the Renin-angiotensin System and Synthesize Angiotensin II. *Gastroenterology* **2003**, *125*, 117–125.
40. Lee, J. I.; Lee, K. S.; Paik, Y. H.; Nyun Park, Y.; Han, K. H.; Chon, C. Y.; Moon, Y. M. Apoptosis of Hepatic Stellate Cells in Carbon Tetrachloride Induced Acute Liver Injury of the Rat: Analysis of Isolated Hepatic Stellate Cells. *J. Hepatol.* **2003**, *39*, 960–966.
41. Huang, Z.; Zhang, Z.; Jiang, Y.; Zhang, D.; Chen, J.; Dong, L.; Zhang, J. Targeted Delivery of Oligonucleotides into Tumor-associated Macrophages for Cancer Immunotherapy. *J. Controlled Release* **2012**, *158*, 286–292.
42. Mencin, A.; Seki, E.; Osawa, Y.; Kodama, Y.; De Minicis, S.; Knowles, M.; Brenner, D. A.; Alpha-1 Antitrypsin, Z. Protein (PiZ) Increases Hepatic Fibrosis in a Murine Model of Cholestasis. *Hepatology* **2007**, *46*, 1443–1452.